



Cite this: *Chem. Sci.*, 2025, **16**, 11481

All publication charges for this article have been paid for by the Royal Society of Chemistry

Received 15th December 2024

Accepted 20th May 2025

DOI: 10.1039/d4sc08472a

[rsc.li/chemical-science](http://rsc.li/chemical-science)

## Introduction

Sugar-receptor interactions are known to mediate a number of biological processes.<sup>1–3</sup> A representative example is the selective interaction between the asialoglycoprotein receptor (ASGPr) and glycoconjugates bearing galactosyl (Gal) or *N*-acetyl-galactosaminyl (GalNAc) residues, which leads to cell endocytosis.<sup>4</sup> ASGPr has been determined to be highly expressed in hepatocytes.<sup>5</sup> Previous studies suggest that ASGPr exhibits important biological functions including disruption of cholesterol metabolism,<sup>6</sup> alleviation of liver injury<sup>7,8</sup> and degradation of serum glycoproteins.<sup>9–11</sup>

*Key Laboratory for Advanced Materials and Joint International Research Laboratory of Precision Chemistry and Molecular Engineering, Feringa Nobel Prize Scientist Joint, Research Center, School of Chemistry and Molecular Engineering, East China University of Science and Technology, 130 Meilong Rd, Shanghai 200237, China.*  
E-mail: [xphe@ecust.edu.cn](mailto:xphe@ecust.edu.cn); [cwang@ecust.edu.cn](mailto:cwang@ecust.edu.cn)

*The International Cooperation Laboratory on Signal Transduction, Eastern Hepatobiliary Surgery Hospital, National Center for Liver Cancer, Shanghai 200438, China*

*National Center for Drug Screening, State Key Laboratory of Drug Research, Shanghai Institute of Materia Medica, Chinese Academy of Sciences, Shanghai 201203, China.*  
E-mail: [jli@simm.ac.cn](mailto:jli@simm.ac.cn)

<sup>a</sup>*Department of Chemistry, University of Bath, Bath BA2 7AY, UK*

<sup>b</sup>*School of Chemistry and Chemical Engineering, Henan Normal University, Xinxiang 453007, China. E-mail: [t.d.james@bath.ac.uk](mailto:t.d.james@bath.ac.uk)*

<sup>†</sup> Electronic supplementary information (ESI) available: Experimental section, additional figures, supplementary movies and original spectra of new compounds. See DOI: <https://doi.org/10.1039/d4sc08472a>

<sup>‡</sup> Equal contribution.

## A BODIPY-tagged trivalent glycocluster for receptor-targeting fluorescence imaging of live cells<sup>†</sup>

Chen Guo,<sup>‡ac</sup> Fang-Yu Si,<sup>‡a</sup> Chen-Han Wang,<sup>‡ab</sup> Ning Wang,<sup>a</sup> Xi-Le Hu,<sup>a</sup> Tony D. James,<sup>ID \*de</sup> Jia Li,<sup>\*c</sup> Chengyun Wang,<sup>ID \*a</sup> and Xiao-Peng He,<sup>ID \*ab</sup>

Multivalent glycoclusters have been extensively used as a targeting agent for drug delivery. However, tools capable of investigating their dynamic interactions with a target receptor remain elusive. Here, we synthesized fluorescently-tagged galactoclusters for the fluorescence imaging of cells that overly express the asialoglycoprotein receptor (ASGPr). A trivalent galactoside was synthesized, to which a boron dipyrromethene (BODIPY) dye was conjugated. The resulting fluorescent glycocluster was used for the targeted fluorescence imaging of liver cancer cells with a high ASGPr expression level. The trivalent probe was also demonstrated to be applicable for super-resolution imaging of ASGPr-mediated ligand endocytosis and the dynamic intracellular translocation to the lysosomes. As such, this study provides a suitable chemical tool for the study of receptor dynamics using fluorescently tagged glycoclusters.

ASGPr has long been exploited as a molecular target for targeted drug delivery. To enhance the receptor-binding avidity, multivalent glycoclusters have been designed and synthesized. Considering the trimeric nature of ASGPr, a variety of trivalent Gal and GalNAc-based glycoclusters have been developed and used for conjugation with therapeutics for targeted drug delivery.<sup>12</sup> For example, several GalNAc-conjugated small-interfering RNA (siRNA) therapeutics have been approved by the FDA.<sup>13–15</sup> Bertozzi *et al.* developed lysosome-targeting chimeras (LYTACs), a novel protein degradation strategy exploiting sugar receptors including ASGPr to mediate endocytosis of membrane-bound proteins.<sup>16</sup> Furthermore, by targeting ASGPr, small-molecule drugs such as docetaxel<sup>17</sup> and immuno-virotherapeutics such as oncolytic herpes simplex virus<sup>18</sup> have been delivered to liver cancer cells in a target-specific manner.

A survey of literature also indicates extensive interest in the development of fluorescent glycoprobes for targeted imaging of live cells and animals. Yan *et al.* synthesized a Gal-conjugated amphiphilic small molecular dye, which can form multivalent nanoparticles in aqueous solution, for NIR-II imaging-guided photothermal therapy (PTT) of liver cancer cells.<sup>19</sup> Wang *et al.* developed Gal-conjugated fluorescent probes for the targeted detection of Fe<sup>3+</sup> in the lysosomes of hepatocytes.<sup>20</sup> Xing *et al.* designed lactosylated fluorescent prodrugs that self-assemble into multivalent nanoparticles for photodynamic therapy and chemotherapy of liver cancer.<sup>21,22</sup> The same group also constructed aggregation-induced emission (AIE)-active fluorescent nanoparticles bearing multiple copies of glucosamine, mannose or sialic acid for the inhibition of insulin fibrillation.<sup>23</sup> We have also developed series of fluorescent dye-conjugated



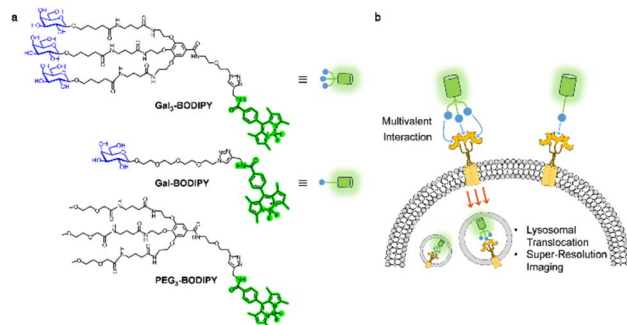


Fig. 1 (a) Chemical structures of **Gal<sub>3</sub>-BODIPY**, **Gal-BODIPY** and **PEG<sub>3</sub>-BODIPY**. (b) Schematic illustration of receptor-targeting cell imaging.

glycoprobes<sup>24–26</sup> and glycoclusters<sup>27–33</sup> for targeted imaging and therapy of bacterial infection as well as cancer. Despite the rapid development of glycocluster-based delivery systems, fluorescent tools capable of tracking glycocluster–receptor interactions remain elusive.

Here, we developed boron dipyrromethene (BODIPY) tagged galactoclusters for the multimodal fluorescence imaging of live cells that overly express ASGPr (Fig. 1). Owing to the unique photophysical properties of BODIPY, we were able to achieve the visualization of the glycoclusters upon cell endocytosis and their dynamic translocation to the lysosomes *via* super-resolution imaging techniques. This offers scope for the monitoring of receptor dynamics upon sugar-receptor interactions.

## Results and discussion

The synthesis of the glycocluster is detailed in Schemes S1 and S2.† Gallic acid was used as a template, on which three molecules of galactose (Gal) were displayed. Three *tert*-butoxycarbonyl-protected alkylamines were first introduced to the phenolic positions of gallic acid, and then an azido poly(ethylene glycol) (PEG) was coupled with the carboxylic group of the template through an amidation reaction. After removal of the Boc groups, three pentanoic acid-modified per-O-acetyl-1-O- $\beta$ -galactosides were coupled to the template through amide bonds. Finally, reaction with an alkynyl BODIPY derivative *via* Cu(i)-catalyzed azide–alkyne cycloaddition reaction, and removal of the acetyl protecting groups resulted in the desired product **Gal<sub>3</sub>-BODIPY** being obtained. A monovalent probe (**Gal-BODIPY**) was synthesized as control with just one galactosyl group introduced to the BODIPY. Another control compound (**PEG<sub>3</sub>-BODIPY**) where the Gal groups were replaced with methyl groups was also synthesized in a similar manner.

With the glycocluster in hand, we determined its photophysical properties. To our delight, the glycocluster is well soluble in phosphate buffered saline (PBS). Therefore, the absorption and fluorescence emission spectra for **Gal<sub>3</sub>-BODIPY** (Fig. 2a), **PEG<sub>3</sub>-BODIPY** (Fig. 2b) and **Gal-BODIPY** (Fig. S1†) were readily obtained. A quantum yield of 0.49 and a lifetime of 1.4 ns was determined for **Gal<sub>3</sub>-BODIPY** in PBS (Table S1†). In

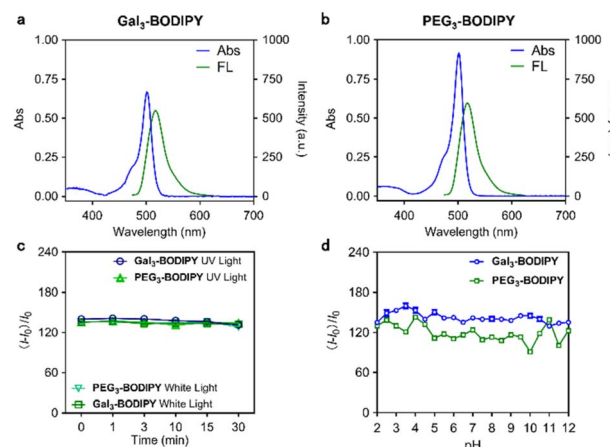


Fig. 2 Absorption (40  $\mu$ M) and fluorescence emission (10  $\mu$ M,  $\lambda_{ex} = 488$  nm) spectra of (a) **Gal<sub>3</sub>-BODIPY** and (b) **PEG<sub>3</sub>-BODIPY** measured in PBS buffer (0.01 M, pH 7.4) (c) fluorescence changes of **Gal<sub>3</sub>-BODIPY** (10  $\mu$ M) and **PEG<sub>3</sub>-BODIPY** (10  $\mu$ M) in PBS buffer (0.01 M, pH 7.4) under white light (560 nm, 1 W cm<sup>-2</sup>) and UV light (365 nm, 1 W cm<sup>-2</sup>) irradiation with time. (d) Fluorescence changes of **Gal<sub>3</sub>-BODIPY** (5  $\mu$ M) and **PEG<sub>3</sub>-BODIPY** (5  $\mu$ M) in 21 different pH PBS buffers (0.01 M, pH 2–12). The slit width was set as 5 nm.

addition, the fluorescence of the glycocluster was not compromised by continuous light irradiation for up to 30 min (Fig. 2c) or exposure to a wide range of pH conditions (Fig. 2d). These results suggest that the BODIPY-tagged glycocluster is suitable for cellular imaging applications.

Next, we turned our attention to evaluate the applicability of the fluorescent glycocluster for targeted cell imaging. Six cell lines including HepG2 (human hepatoma cell), Huh7 (human hepatoma cell), MHCC-97H (human hepatoma cell), MDA-MB-231 (human triple-negative breast cancer cell), HeLa (human cervical cancer cell) and RAW264.7 (mouse macrophage cell) with different ASGPr expression levels were used (HepG2, Huh7, MDA-MB-231, HeLa and RAW264.7 cell lines were purchased from American Type Culture Collection (ATCC), and MHCC-97H cell line was purchased from National Collection of Authenticated Cell Cultures). First the quantitative polymerase chain reaction was first used to determine the relative ASGPr mRNA level of all six cell lines. Then, cells were incubated with **Gal<sub>3</sub>-BODIPY**, **PEG<sub>3</sub>-BODIPY** or **Gal-BODIPY**, and imaged by a high-content screening system. We determined that the fluorescence of **Gal<sub>3</sub>-BODIPY** was stronger in HepG2 than in other cells (Fig. 3a and b). The quantified fluorescence intensity of the probe agreed with the endogenous ASGPr expression level of the cells (Fig. 3c). Interestingly, the fluorescence intensity of **Gal-BODIPY** in all the tested cells was seen to be constantly smaller than that of **Gal<sub>3</sub>-BODIPY**, suggesting a stronger binding between the trivalent ligand and ASGPr. This agrees with the observation in a previous study.<sup>34</sup> In contrast, a similar level of fluorescence was detected in all six cells for **PEG<sub>3</sub>-BODIPY** without Gal modification (Fig. 3a and b). We also determined that the fluorescence imaging of HepG2 cells by **Gal<sub>3</sub>-BODIPY** was concentration (Fig. S2†) and time-dependent (Fig. S2†), and that the glycocluster was not toxic to the cells



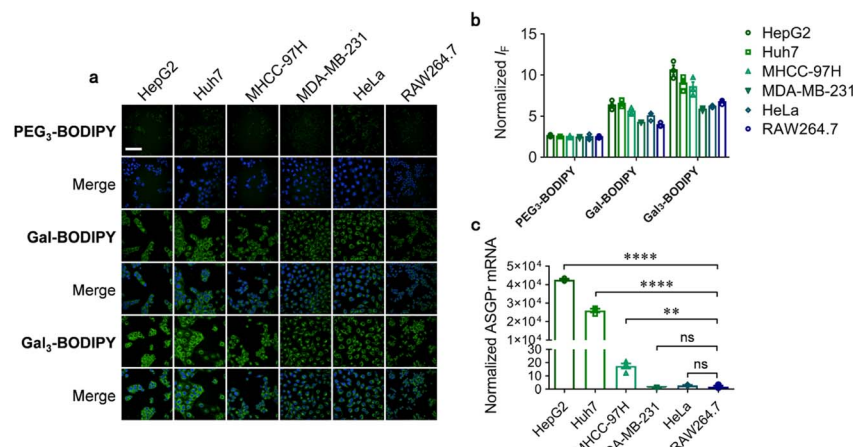


Fig. 3 (a) Fluorescence imaging and (b) quantification of HepG2, Huh7, MHCC-97H, MDA-MB-231, HeLa and RAW264.7 cells after treatment with Gal<sub>3</sub>-BODIPY (5  $\mu$ M), PEG<sub>3</sub>-BODIPY (5  $\mu$ M) or Gal-BODIPY (5  $\mu$ M) for 1 h. (c) ASGPr mRNA expression level of the cell lines used for imaging measured by RT qPCR (scale bar = 100  $\mu$ m).

tested (Fig. S3†). These results help confirm the ASGPr-targeting ability of Gal<sub>3</sub>-BODIPY.

To corroborate that the targeted imaging is receptor-dependent, several other experiments were carried out. RNA interference was carried out to suppress the ASGPr expression level in HepG2 cells (Fig. 4c). We determined that cells treated with ASGPr siRNA exhibited a significantly lower cellular uptake of the glycoclusters than those without siRNA treatment (Fig. 4a and b). Incubation of HepG2 cells with Gal<sub>3</sub>-BODIPY at 4 °C significantly decreased the fluorescence intensity with respect to 37 °C incubation (Fig. 4d and e), suggesting the internalization of the glycocluster is kinetically controlled.<sup>35</sup> In addition, preincubation of the cells with an excess of free Gal suppressed the fluorescence of the glycocluster (Fig. 4f and g).

With promising imaging results obtained, we set out to examine the applicability of the BODIPY-tagged glycocluster for

multimodal cell imaging. BODIPY is a class of popular organic dyes often used for live cell imaging because of its high brightness and amenability for super-resolution imaging.<sup>36–39</sup> We used a Leica STELLARIS 8 STED (stimulated emission depletion) system to image HepG2 cells after incubation with 10  $\mu$ M of Gal<sub>3</sub>-BODIPY for 5 min under STED and confocal mode (Fig. S4†). With STED, we obtained fluorescence images with suppressed background signals and higher resolution compared to the confocal images. We then set out to explore the super-resolution imaging of ASGPr-mediated endocytic processes using Gal<sub>3</sub>-BODIPY. Ly-Red-BODIPY, a lysosomal tracker developed in our laboratory was used for this experiment (Scheme S3 and Fig. S5†).

HepG2 and HeLa cells pre-incubated with Ly-Red-BODIPY were treated with Gal<sub>3</sub>-BODIPY and then imaged every 30 s (Fig. 5). During an imaging period of 300 s, we observed that

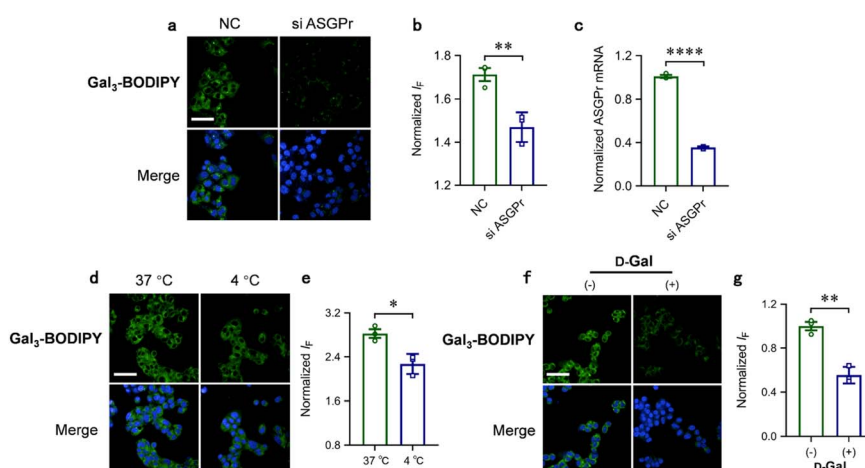


Fig. 4 (a) Fluorescence imaging, (b) quantification and (c) mRNA expression level of ASGPr knock-down HepG2 cells and relative control cells. (d) Fluorescence imaging and (e) quantification of Gal<sub>3</sub>-BODIPY cultured HepG2 cells at different temperature. (f) Fluorescence imaging and (g) quantification of HepG2 cells preincubated with free D-galactose (scale bar = 100  $\mu$ m). BODIPY channel excitation at 488 nm, emission at 500–550 nm. Hoechst 33342 channel excitation at 405 nm, emission at 435–480 nm.



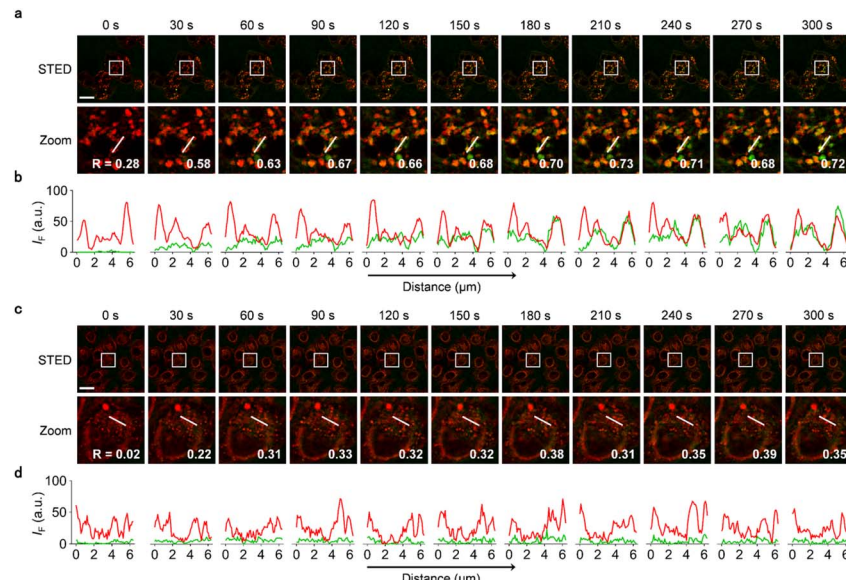


Fig. 5 (a) Fluorescence imaging and (b) linear quantification of HepG2 cells incubated with  $\text{Gal}_3\text{-BODIPY}$  and Ly-Red-BODIPY under STED mode. The Zoom images are those enlarged from the white boxes shown in the STED images. (c) Fluorescence imaging and (d) linear quantification of HeLa cells incubated with  $\text{Gal}_3\text{-BODIPY}$  and Ly-Red-BODIPY under STED mode. BODIPY channel: excitation at 488 nm, emission at 500–550 nm and depletion with 775 nm STED laser. Ly-Red-BODIPY channel: excitation at 638 nm, emission at 640–700 nm and depletion with 775 nm STED laser. Green and red lines represent the fluorescence intensity of  $\text{Gal}_3\text{-BODIPY}$  and that of Ly-Red-BODIPY, respectively. The corresponding Pearson's Correlation Coefficient is labelled in the bottom-right (scale bar = 25  $\mu\text{m}$ ).

$\text{Gal}_3\text{-BODIPY}$  was rapidly internalized by HepG2 cells from 0–30 s and translocated to the lysosomes immediately. Then, the probes resided in the lysosomes over the complete imaging cycle as evidenced by its high Pearson's coefficient values determined when overlapped with **Ly-Red-BODIPY** (Fig. 5a and b, and ESI movie 1†). In contrast,  $\text{Gal}_3\text{-BODIPY}$  was hardly internalized by HeLa cells under the same imaging conditions, and a low overlap between the fluorescence of the probe and that of the lysosomal tracker was determined (Fig. 5c, d, and ESI movie 2†). In the meantime,  $\text{PEG}_3\text{-BODIPY}$  used as a control was found to be barely internalized by both HepG2 and HeLa cell lines (Fig. S6†), which agrees with the results obtained by high-content fluorescence imaging. We also found that  $\text{Gal}_3\text{-BODIPY}$  was applicable for lifetime imaging, and a lifetime of 3.98 ns was determined for the probe (Fig. S7†). This indicates that BODIPY-modified glycoclusters can be used for lifetime imaging of ASGPr-mediated endocytosis.

## Conclusions

We have synthesized a BODIPY-tagged galactocluster for targeted imaging of live cells. A gallic acid-based tripod was used to display three molecules of Gal, and the resulting trivalent glycocluster was shown to be selectively internalized by cells that overly express ASGPr. In addition, the unique photophysical properties of BODIPY enabled us to visualize ASGPr-mediated endocytosis and intracellular translocation to the lysosomes using super-resolution imaging techniques. This study offers insights for the elaboration of receptor dynamics in live cells using BODIPY-tagged glycoclusters.

## Data availability

All data generated during this study have been included as part of the ESI.†  $^1\text{H}$  and  $^{13}\text{C}$ -NMR spectra for unreported compounds can be found in the ESI.†

## Author contributions

T. D. J., J. L., C.-Y. W. and X.-P. H. designed research; C. G., F.-Y. S., C.-H. W. and N. W. performed research; X.-L. H., T. D. J. and X.-P. H. wrote the paper.

## Conflicts of interest

The authors declare no conflict of interest.

## Acknowledgements

The authors thank the Natural National Science Foundation of China (NSFC) (No. 92253306, 82130099 and 22477030), Science and Technology Commission of Shanghai Municipality (grant No. 24DX1400200), the International Cooperation Program of Shanghai Science and Technology (No. 23490711600), the Fundamental Research Funds for the Central Universities (222201717003), the Programme of Introducing Talents of Discipline to Universities (B16017), the National Natural Science Foundation of Shanghai Science and Technology (No. 24ZR1415400), the Shanghai Oriental Talents youth Program (No. QNKJ2024010), the Shanghai Xuhui District Hospital Local Cooperation Project (23XHYD-20), the Open Funding Project of the State Key Laboratory of Fine Chemicals, Dalian University of



Technology (KF 2402), State Key Laboratory of Chemo/Biosensing and Chemometrics, Hunan University, Changsha 410082, P. R. China, Ministry of Education Key Laboratory on signaling Regulation and Targeting Therapy of Liver Cancer (Naval Medical University) (Grant. 2023-MEKLLC-MS/ZD-00\*) and Shandong Laboratory Program (SYS202205) for financial support. T. D. J. wishes to thank the University of Bath and the Open Research Fund of the School of Chemistry and Chemical Engineering, Henan Normal University (2020ZD01) for support. The Research Center of Analysis and Test of East China University of Science and Technology was gratefully acknowledged for assistance in analytical experiments.

## Notes and references

- 1 S. S. Pinho, I. Alves, J. Gaifem and G. A. Rabinovich, *Cell. Mol. Immunol.*, 2023, **20**, 1101–1113.
- 2 B. a. H. Smith and C. R. Bertozzi, *Nat. Rev. Drug Discovery*, 2021, **20**, 217–243.
- 3 T. Johannsson and B. Lepenies, *Trends Biotechnol.*, 2016, **35**, 334–346.
- 4 A. A. D'Souza and P. V. Devarajan, *J. Controlled Release*, 2015, **203**, 126–139.
- 5 H. J. Geuze, J. W. Slot, G. J. A. M. Strous, J. Peppard, K. Von Figura, A. Hasilik and A. L. Schwartz, *Cell*, 1984, **37**, 195–204.
- 6 J.-Q. Wang, L.-L. Li, A. Hu, G. Deng, J. Wei, Y.-F. Li, Y.-B. Liu, X.-Y. Lu, Z.-P. Qiu, X.-J. Shi, X. Zhao, J. Luo and B.-L. Song, *Nature*, 2022, **608**, 413–420.
- 7 Z. Zhang, X. K. Leng, Y. Y. Zhai, X. Zhang, Z. W. Sun, J. Y. Xiao, J. F. Lu, K. Liu, B. Xia, Q. Gao, M. Jia, C. Q. Xu, Y. N. Jiang, X. G. Zhang, K. S. Tao and J. W. Wu, *Nat. Commun.*, 2024, **15**, 1908.
- 8 C. A. Casey, A. J. Macke, R. R. Gough, A. N. Pachikov, M. E. Morris, P. G. Thomas, J. L. Kubik, M. S. Holzapfel and A. Petrosyan, *Hepatol. Commun.*, 2021, **6**, 374–388.
- 9 W. H. Yang, P. V. Aziz, D. M. Heithoff, M. J. Mahan, J. W. Smith and J. D. Marth, *Proc. Natl. Acad. Sci. U. S. A.*, 2015, **112**, 13657–13662.
- 10 B. Huang, M. Abedi, G. Ahn, B. Coventry, I. Sappington, C. Tang, R. Wang, T. Schlichthaerle, J. Z. Zhang, Y. Wang, I. Goreshnik, C. W. Chiu, A. Chazin-Gray, S. Chan, S. Gerben, A. Murray, S. Wang, J. O'Neill, L. Yi, R. Yeh, A. Misquith, A. Wolf, L. M. Tomasovic, D. I. Piraner, M. J. D. Gonzalez, N. R. Bennett, P. Venkatesh, M. Ahlrichs, C. Dobbins, W. Yang, X. Wang, D. D. Sahtoe, D. Vafeados, R. Mout, S. Shivaei, L. Cao, L. Carter, L. Stewart, J. B. Spangler, K. T. Roybal, P. J. Greisen, X. Li, G. J. L. Bernardes, C. R. Bertozzi and D. Baker, *Nature*, 2025, **638**, 796–804.
- 11 D. F. Caianiello, M. Zhang, J. D. Ray, R. A. Howell, J. C. Swartzel, E. M. J. Branham, E. Chirkin, V. R. Sabbasani, A. Z. Gong, D. M. McDonald, V. Muthusamy and D. A. Spiegel, *Nat. Chem. Biol.*, 2021, **17**, 947–953.
- 12 V. Kumar and W. B. Turnbull, *Chem. Soc. Rev.*, 2023, **52**, 1273–1287.
- 13 V. Jadhav, A. Vaishnav, K. Fitzgerald and M. A. Maier, *Nat. Biotechnol.*, 2024, **42**, 394–405.
- 14 B. Hu, L. Zhong, Y. Weng, L. Peng, Y. Huang, Y. Zhao and X.-J. Liang, *Signal Transduction Targeted Ther.*, 2020, **5**, 101.
- 15 Y. N. Lamb, *Drugs*, 2021, **81**, 389.
- 16 G. Ahn, S. M. Banik, C. L. Miller, N. M. Riley, J. R. Cochran and C. R. Bertozzi, *Nat. Chem. Biol.*, 2021, **17**, 937–946.
- 17 R. A. Petrov, S. R. Mefedova, E. Yu. Yamansarov, S. Yu. Maklakova, D. A. Grishin, E. V. Lopatukhina, O. Y. Burenina, A. V. Lopukhov, S. V. Kovalev, Y. V. Timchenko, E. E. Ondar, Y. A. Ivanenkov, S. A. Evteev, A. N. Vaneev, R. V. Timoshenko, N. L. Klyachko, A. S. Erofeev, P. V. Gorelkin, E. K. Beloglazkina and A. G. Majouga, *Mol. Pharm.*, 2020, **18**, 461–468.
- 18 Y. Liang, B. Wang, Q. Chen, X. Fu, C. Jiang, Z. Lin, Q. Zhuang, Y. Zeng, X. Liu and D. Zhang, *Theranostics*, 2023, **13**, 5452–5468.
- 19 H. Dang, Y. Tian, Q. Cheng, C. Teng, K. Xie and L. Yan, *J. Colloid Interface Sci.*, 2021, **612**, 287–297.
- 20 Y. Wang, F. Liu, C. Pu, Z. Tong, M. Wang and J. Wang, *Biosens. Bioelectron.*, 2022, **204**, 114083.
- 21 W. Zhou, Y.-C. Liu, G.-J. Liu, Y. Zhang, G.-L. Feng and G.-W. Xing, *Angew. Chem. Int. Ed. Engl.*, 2024, e202413350.
- 22 Y. Liu, G. Liu, W. Zhou, G. Feng, Q. Ma, Y. Zhang and G. Xing, *Angew. Chem. Int. Ed. Engl.*, 2023, **62**, e202309786.
- 23 Y.-M. Ji, W. Zhang, J.-D. Zhang, X.-F. Li, F.-D. Yu, C.-Y. Li, G.-J. Liu and G.-W. Xing, *J. Mater. Chem. B*, 2022, **10**, 5602–5611.
- 24 Y.-H. Wu, G.-J. Wang, C. Guo, P.-P. Wang, J.-Y. Wang, X.-L. Hu, Y. Zang, T. D. James, J. Li and X.-P. He, *Chem. Commun.*, 2024, **60**, 8240–8243.
- 25 X. Chai, H.-H. Han, A. C. Sedgwick, N. Li, Y. Zang, T. D. James, J. Zhang, X.-L. Hu, Y. Yu, Y. Li, Y. Wang, J. Li, X.-P. He and H. Tian, *J. Am. Chem. Soc.*, 2020, **142**, 18005–18013.
- 26 J. Zhang, Y. Fu, H.-H. Han, Y. Zang, J. Li, X.-P. He, B. L. Feringa and H. Tian, *Nat. Commun.*, 2017, **8**, 987.
- 27 X.-L. Hu, H.-Q. Gan, W.-Z. Gui, K.-C. Yan, J. L. Sessler, D. Yi, H. Tian and X.-P. He, *Proc. Natl. Acad. Sci. U. S. A.*, 2024, **121**, 2408716121.
- 28 Y. Shang, S. Zhang, H.-Q. Gan, K.-C. Yan, F. Xu, Y. Mai, D. Chen, X.-L. Hu, L. Zou, T. D. James and X.-P. He, *Chem. Commun.*, 2023, **59**, 1094–1097.
- 29 L. Dong, M.-Y. Zhang, H.-H. Han, Y. Zang, G.-R. Chen, J. Li, X.-P. He and S. Vidal, *Chem. Sci.*, 2021, **13**, 247–256.
- 30 H.-N. Xie, Y.-Y. Chen, G.-B. Zhu, H.-H. Han, X.-L. Hu, Z.-Q. Pan, Y. Zang, D.-H. Xie, X.-P. He, J. Li and T. D. James, *Chem. Commun.*, 2022, **58**, 5029–5032.
- 31 C. Zhang, D.-T. Shi, K.-C. Yan, A. C. Sedgwick, G.-R. Chen, X.-P. He, T. D. James, B. Ye, X.-L. Hu and D. Chen, *Nanoscale*, 2020, **12**, 23234–23240.
- 32 W.-T. Dou, Z.-Y. Qin, J. Li, D.-M. Zhou and X.-P. He, *Sci. Bull.*, 2019, **64**, 1902–1909.
- 33 X.-L. Hu, Q. Cai, J. Gao, R. A. Field, G.-R. Chen, N. Jia, Y. Zang, J. Li and X.-P. He, *ACS Appl. Mater. Interfaces*, 2019, **11**, 22181–22187.



34 R. A. Petrov, S. R. Mefedova, E. Yu Yamansarov, S. Yu Maklakova, D. A. Grishin, E. V. Lopatukhina, O. Y. Burenina, A. V. Lopukhov, S. V. Kovalev, Y. V. Timchenko, E. E. Ondar, Y. A. Ivanenkov, S. A. Evteev, A. N. Vaneev, R. V. Timoshenko, N. L. Klyachko, A. S. Erofeev, P. V. Gorelkin, E. K. Beloglazkina and A. G. Majouga, *Mol. Pharm.*, 2020, **18**, 461–468.

35 P. H. Weigel and J. A. Oka, *J. Biol. Chem.*, 1981, **256**, 2615–2617.

36 S. Pim, A. C. Bourgès, D. Wu, G. Durán-Sampedro, M. Garre and D. F. O'Shea, *Chem. Sci.*, 2024, **15**, 14913–14923.

37 C. S. Wijesooriya, J. A. Peterson, P. Shrestha, E. J. Gehrmann, A. H. Winter and E. A. Smith, *Angew. Chem. Int. Ed. Engl.*, 2018, **57**, 12685–12689.

38 L. Saladin, V. Breton, V. L. Berruyer, P. Nazac, T. Lequeu, P. Didier, L. Danglot and M. Collot, *J. Am. Chem. Soc.*, 2024, **146**, 17456–17473.

39 Y. Xu, T. Feng, T. Yang, H. Wei, H. Yang, G. Li, M. Zhao, S. Liu, W. Huang and Q. Zhao, *ACS Appl. Mater. Interfaces*, 2018, **10**, 16299–16307.

